crystals

MDPI

Article

PS/Al-μPs Surface Modification for Enhanced Optical and Electronic Performance of Multicrystalline Silicon

Yasmin Zouari [1,2], Achraf Manai [1], Rabia B. Zaghouani [3], Karim Choubani [4,*], Mohammed A. Almeshaal [4], Wissem Dimassi [1] and Mohamed Ben Rabha [1]

[1] Laboratoire de Nanomatériaux et Systèmes Pour Énergies Renouvelables, Centre de Recherches et des Technologies de l'Énergie, Technopôle de Borj Cédria, BP 95 Hammam-Lif, Tunis 2050, Tunisia; yazou2001@gmail.com (Y.Z.); achref.mannai87@gmail.com (A.M.); dimassi.wissem@gmail.com (W.D.); rabha2222@yahoo.fr (M.B.R.)
[2] Département de Physique, Faculté des Sciences, Universite de Tunis el Manar, BP 94, Rommana, Tunis 1068, Tunisia
[3] Laboratoire de Photovoltaïque, Centre de Recherches et des Technologies de l'Energie, Technopôle de Borj Cédria, BP 95 Hammam-Lif, Tunis 2050, Tunisia; rabia.benabderrahmane@gmail.com
[4] College of Engineering, Imam Mohammad Ibn Saud Islamic University (IMSIU), Riyadh 11432, Saudi Arabia; maalmeshaal@imamu.edu.sa
* Correspondence: kelchobani@imamu.edu.sa

Abstract

In this paper, we report on the effect of combining porous silicon with aluminum microparticles (PS/Al-μPs) on the optical and electronic properties of multicrystalline silicon (mc-Si). An aluminum film was deposited on the mc-Si surface, annealed at 750 °C for 20 min, and partially remained on the surface after CP_4 treatment. The surface was subsequently treated with a stain-etching solution ($HF/HNO_3/H_2O$) to form a porous silicon (PS) layer. The resulting mc-Si with PS/Al-μPs modification led to a marked improvement in the optoelectronic performance of the treated mc-Si. Surface reflectance was reduced from 34.6% to 9.1% across 400–800 nm wavelength range, corresponding to a 74% decrease. Minority carrier lifetime increased from 2 μs in untreated samples to 1 ms after Al-μPs passivation and remained elevated at 285 μs following stain etching. Additionally, the effective surface recombination velocity dropped from 50 $cm{\cdot}s^{-1}$ to 0.35 $cm{\cdot}s^{-1}$ and a reduction in [Fe] after treatment confirms the effectiveness of the PS-Al-μPs gettering process. FTIR analysis confirmed the formation of Si–H and Al–O bonds, highlighting effective surface passivation and suppression of recombination losses.

Keywords: mc-Si; aluminum microparticles; porous silicon; carrier lifetime; surface recombination velocity; passivation

Check for updates

Academic Editor: Giancarlo Salviati

Received: 13 February 2026
Revised: 10 April 2026
Accepted: 21 April 2026
Published: 19 May 2026

Copyright: © 2026 by the authors. Licensee MDPI, Basel, Switzerland. This article is an open access article distributed under the terms and conditions of the Creative Commons Attribution (CC BY) license.

1. Introduction

The increasing global energy demand, along with the urgent need to reduce carbon emissions, has established solar photovoltaics (PV) as a key technology for sustainable energy generation [1–3]. Producing high-efficiency solar cells requires high-purity silicon, as impurities can significantly reduce carrier lifetime and overall device performance. Multicrystalline silicon (mc-Si) dominates the PV market [4,5], accounting for nearly 90% of production due to its reliability, relatively low manufacturing cost, and long operational lifetime. However, its performance is often limited by defects and grain boundaries [6–9], which act as recombination centers and reduce carrier collection efficiency. To address these challenges, effective surface passivation and defect mitigation strategies are essential. The

electronic quality of multicrystalline silicon (mc-Si) has significantly improved in recent years through surface passivation [10–13], which remove or immobilize impurities and defects from the device-active regions, thereby enhancing the minority carrier diffusion length and overall solar cell efficiency. Gettering is a well-established purification method that enhances the electronic quality of silicon by extracting metallic impurities from electrically active regions and redistributing them to designated sink sites. Conventional gettering approaches, including phosphorus diffusion gettering [14], have been reported to provide modest improvements in minority carrier lifetime, reaching values of approximately 140 μs. In addition, aluminum-assisted gettering [15,16] has been shown to significantly improve the electronic quality of silicon by removing metallic impurities and reducing recombination centers. For example, the incorporation of an aluminum/porous silicon structure can increase the effective minority carrier lifetime to values exceeding 100 μs, compared with a reference lifetime of approximately 2 μs in untreated samples. These results highlight the effectiveness of aluminum-based gettering techniques in enhancing the electrical quality of silicon materials. Also, silicon nitride-based gettering [17–19] is typically implemented during high-temperature thermal treatments and effectively improves carrier transport and lifetime. However, these processes have a limited impact on surface reflectivity, necessitating complementary strategies to reduce optical losses. Emerging approaches using aluminum (Al) and porous silicon (PS) have proven effective in simultaneously providing surface passivation and anti-reflective benefits. PS, formed via acid-based stain etching, lowers surface reflectivity and enables hydrogen diffusion, which further passivates surface defects [20,21]. At the same time, aluminum diffuses along the wafer surface, forms traps for recombination-active impurities [22], and facilitates their dissolution, an effect partially attributed to the activation of internal getters and the formation of impurity complexes.

In this study, we investigate stain-etching-derived PS in the presence of aluminum microparticles (Al-μPs) and assess its impact on surface morphology, optical behavior, and minority carrier lifetime, providing insights into the synergistic enhancement of both bulk and surface electronic quality in mc-Si solar cells. In this work, we investigate the effect of PS/Al-μPs surface modification on mc-Si, including changes in surface reflectance, carrier lifetime, and surface recombination velocity, providing insights into improving the electronic quality of multicrystalline silicon solar cells.

2. Experimental

All experiments were performed on p-type multicrystalline silicon (mc-Si) wafers with a thickness of 200 μm and a resistivity in the range of 0.5–2 Ω·cm. An 8 μm thick aluminum layer was deposited on the wafer surface by screen printing using an aluminum paste. After deposition, the layer was carefully dried to remove solvents and ensure uniform coverage. The wafers were then subjected to a high-temperature annealing process at 750 °C for 20 min, which promoted aluminum diffusion into the silicon grains and along the grain boundaries, forming a uniform aluminum–silicon alloy that enhances electrical contact and passivation of the substrate. Subsequently, the mc-Si surface was chemically treated in a $HF/HNO_3/H_2SO_4$ (1:3:5) solution for a few seconds to partially remove the continuous aluminum layer, resulting in the formation of Al-μPs on the silicon surface. The resulting mc-Si/Al-MPs samples were then subjected to a stain-etching process using a $HF/HNO_3/H_2O_2$ solution to generate PS nanostructures [23]. Chemical etching was carried out on mc-Si/Al-μPs wafers with a surface area of 1.5 × 1.5 cm^2, employing an optimized immersion time of 6 min at 25 °C in a solution composed of HF (48 wt%)/HNO_3 (65 wt%)/H_2O_2 with a volume ratio of 1:2:4. This process enabled the formation of a porous silicon layer on the mc-Si/Al-μPs surface. Immediately after etching, the samples

were thoroughly rinsed with deionized water and dried under a nitrogen flow to prevent degradation of the porous silicon layer.

The morphological characteristics of multicrystalline silicon (mc-Si) surfaces after Al-μPs deposition and PS/Al-μPs processing was examined using scanning electron microscopy (JEOL JSM-5400, Tokyo, Japan) to investigate roughness and pore development. The optical behavior of the modified mc-Si samples was studied by measuring reflectance spectra with a LAMBDA 950 UV–Vis–NIR spectrophotometer equipped with an integrating sphere (Perkin-Elmer Lambda 950, Springfield, IL, USA), covering the wavelength range from 300 to 1200 nm. The chemical composition and bonding features of the porous silicon layer were analyzed using Fourier transform infrared (FTIR) spectroscopy (Nicolet MAGNA-IR 560 ESP FT-IR, Nicolet Instrument Corporation, Madison, WI, USA). Additionally, the effective minority carrier lifetime was evaluated using a photoconductance lifetime measurement setup (WCT-120, IPVF, Palaiseau, French) to assess the impact of surface modification on the electronic properties of the samples, and interstitial iron concentration ([Fe]) before and after treatment was generated using a WT-2000PVN Multifunction Wafer Mapping Tool (WT-2000PVN, Semilab, Budapest, Hungary). In addition, several key parameters were experimentally measured and evaluated to assess material quality.

3. Results and Discussion

Figure 1 presents SEM images revealing the surface morphology of the silicon substrate at different magnifications, following the removal of the aluminum layer. The resulting metal microparticles are distributed at varying concentrations along the grain boundary regions of multicrystalline silicon. During subsequent etching, these metal particles guide the formation of pores or macropores on the silicon surface, with their positions corresponding to the locations of the metal deposits [24].

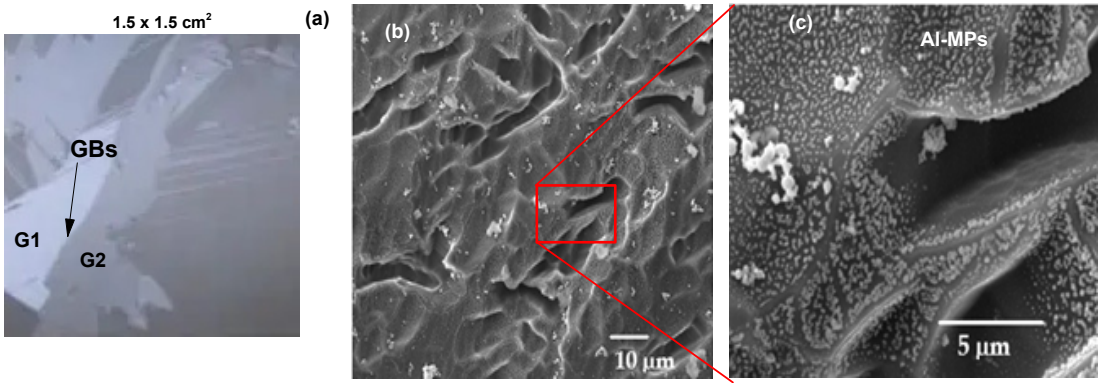

Figure 1. SEM images of (**a**) Ref mc-Si (with G and GBs) and (**b**,**c**) mc-Si of residual Al-μPs.

Scanning electron microscopy (SEM) is a critical tool for characterizing the surface morphology, size distribution, texture, and agglomeration behavior of Al-μPs. Figure 1 shows the surface morphology of multicrystalline silicon (mc-Si) samples illustrating the effect of Al-μPs. Figure 1a shows the surface of the reference mc-Si wafer prior to aluminum treatment, exhibiting a relatively smooth and untreated morphology. The characteristic grain structure, typically ranging from 1 to 10 mm, allows multicrystalline silicon to be easily recognized by the naked eye. Figure 1b,c show the mc-Si surface after Al-μP formation. Figure 1c provides a higher-magnification SEM image of the red-marked region in Figure 1b, revealing a uniform distribution of Al-μPs across the mc-Si surface. These Al-μPs act as effective gettering sites for recombination-active impurities and contribute to improved surface passivation. Owing to their catalytic activity, when the surface is subjected to stain etching, the Al-μPs preferentially promote the reduction in the oxidizing

species at their surface, facilitating localized silicon dissolution and the formation of porous silicon.

The mc-Si substrate with dispersed metal microparticles was immersed in a solution of HF, H_2O_2, and HNO_3 in a 1:4:2 volume ratio. The purpose of this aluminum-assisted treatment is twofold: first, to examine the surface morphology under the original experimental conditions, and second, to evaluate whether the process preserves the electronic quality of the material.

SEM images reveal a spongy, porous structure that supports light-trapping within the silicon surface. Higher-magnification images show that the pores form not only within the Si grains but are more concentrated along the grain boundaries, which helps reduce the impact of defects in the amorphous regions. Additionally, holes are observed on the textured surface, which are attributed to the diffusion of aluminum through silicon during annealing. These surface features can enhance light trapping by promoting multiple internal reflections, due to the depth and geometry of the pores and holes and passivation defects.

Figure 2a,b present SEM images of multicrystalline silicon (mc-Si) of residual aluminum microparticle (Al-µPs) and subsequent stain-etching, leading to porous silicon formation. The right image (Figure 2b) is a magnified view of the region marked by the red square in the left image (Figure 2a), revealing detailed features of the porous structure. Irregularly shaped pores with varying sizes are observed, together with residual Al-µPs located within the porous matrix or near pore edges, indicating partial retention after the etching process. The transformation of the silicon surface into a porous, textured morphology significantly increases both the effective surface area and roughness. This modification enhances light trapping by promoting multiple internal scattering events within the pore network. In addition, the resulting gradual refractive index transition extends the optical path length of incident photons, leading to a noticeable reduction in surface reflectivity [25,26]. Beyond these optical effects, the presence of aluminum after heat treatment contributes to the passivation of surface states and grain boundaries, particularly in multicrystalline silicon. Diffused aluminum helps neutralize dangling bonds and induces field-effect passivation, thereby reducing surface recombination rates. As a result, the minority carrier diffusion length is improved, supporting a more effective balance between light absorption and efficient charge carrier collection [15,16,27]. This combined structural and chemical modification makes the treated mc-Si surface particularly suitable for photovoltaic applications.

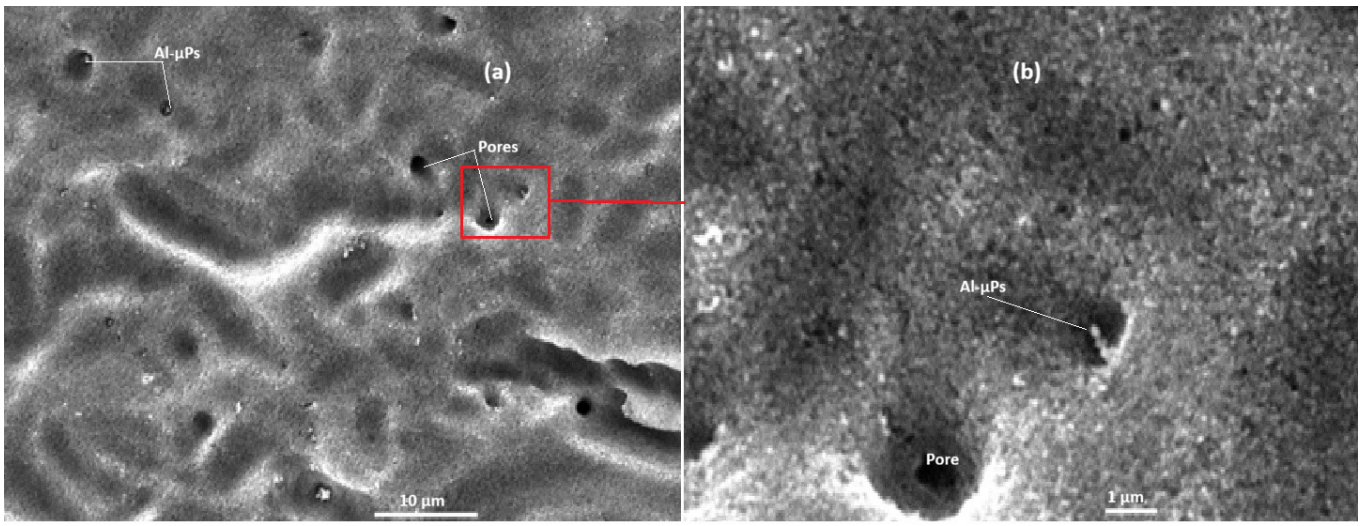

Figure 2. SEM images of mc-Si (**a**) after PS-Al-µPs treatment, and (**b**) magnified view of the region marked by the red square.

An SEM image of mc-Si after PS-Al-μPs treatment was analyzed to determine the size distributions of aluminum particles and silicon pores. The resulting histogram (Figure 3) shows that the Aluminum-Assisted Chemical Etching (AACE) process is not random but closely reflects the geometry of the catalyst. The process exhibits strong localization, with a mean pore size of ~4 μm, matching the typical dimensions of the aluminum clusters. Small pores (<2 μm) are primarily formed by individual aluminum micro-grains, while larger pores (>5 μm) arise from aluminum macro-agglomerates or extended etching times. This demonstrates the direct impact of catalyst morphology and etching conditions on the pore size distribution.

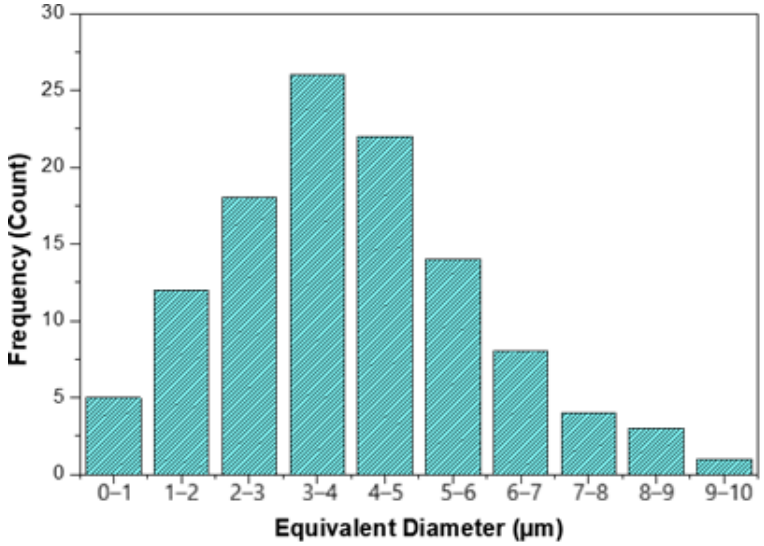

Figure 3. Size distribution of structural elements in Al-etched porous silicon.

The integration of porous silicon (PS) and aluminum microparticles (Al-μPs) creates a synergistic hybrid architecture that optimizes both optical and electrical performance. In this configuration, the nanostructured PS layer serves as a graded refractive index medium, significantly cutting reflectance and boosting photon trapping. Simultaneously, the Al-μPs enhance surface conductivity and provide essential passivation, which minimizes surface recombination velocity and streamlines charge carrier collection. By resolving the inherent tension between light harvesting and charge transport, this composite structure presents a scalable pathway for advancing high-efficiency photovoltaic and optoelectronic technologies.

Figure 4 outlines the Al-Assisted Chemical Etching process. Aluminum catalyzes the reduction of the oxidant, producing holes that are injected into silicon at the metal/Si interface. These holes induce silicon oxidation, followed by its dissolution in HF, resulting in localized etching beneath the metal. Since the hole density is highest at the interface, etching is enhanced in metal-covered regions. If hole generation exceeds consumption, they spread into surrounding areas, promoting additional etching and the possible formation of microporous silicon. The catalytic activity of aluminum is not hindered by oxidation, owing to the dynamic balance between oxide formation and its dissolution by HF. In the etching solution, HF continuously removes the aluminum oxide layer, preventing the buildup of a dense barrier. Even when aluminum particles are partially encapsulated by their native oxide shell, this layer remains sufficiently thin due to HF action and does not impede catalytic activity.

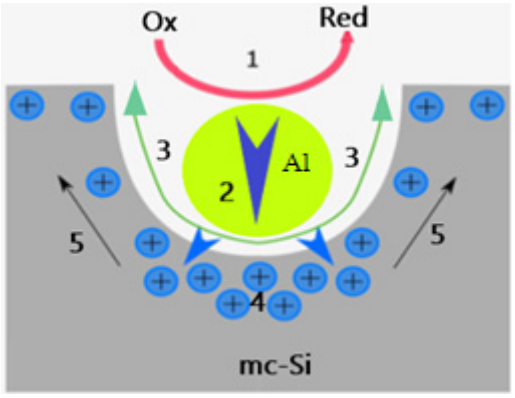

Figure 4. Process diagram of assisted chemical etching metal.

Figure 5 presents the dependence of minority carrier lifetime on excess carrier concentration, as measured using the WCT-120 photoconductance lifetime technique. For untreated multicrystalline silicon, the measurable response is typically limited to carrier concentrations below 10^{15} cm^{-3}. In contrast, aluminum microparticle passivation significantly alters this behavior. During annealing, aluminum diffuses into the silicon, forming an effective P^+-type surface layer that enables carrier concentrations to reach up to 10^{16} cm^{-3}. This modification leads to a significant increase in the minority carrier lifetime compared to unpassivated silicon. At a minority carrier density (Δn) of about 1×10^{15} cm^{-3}, the minority carrier lifetime of untreated mc-Si is approximately 2 µs (Figure 5a). After Al-MPs passivation, the lifetime increases to nearly 1 ms at a minority carrier density (Δn) of about 1×10^{15} cm^{-3} (Figure 5b), indicating a strong reduction in recombination due to aluminum passivation of grains and grain boundaries due to the gettering of recombination-active impurity in mc-Si [22].

Figure 5c illustrates the effect of the $HF/H_2O_2/HNO_3$ treatment on mc-Si/Al-MPs samples. After the $HF/H_2O_2/HNO_3$ treatment, the minority carrier lifetime decreases to about 285 µs at a carrier density (Δn) of approximately 1×10^{15} cm^{-3}. In comparison, the maximum lifetime reported after phosphorus gettering (P-gettering) was around 250 µs [28], reaching values up to 140 µs [14], while hydrogenation of the gettered wafers yielded an effective lifetime of 190 µs [29].

This reduction in lifetime can be mainly attributed to the partial dissolution of the aluminum layer and the development of pores on the silicon surface. Despite this decrease, the treatment generates a sponge-like porous structure that significantly improves light trapping and optical absorption.

The evolution of the effective minority carrier lifetime (τ_{eff}) and the corresponding effective surface recombination velocity (S_{eff}) is summarized in Table 1. The values of S_{eff} were determined from the experimentally measured τ_{eff} using the analytical relationship given in Equation (1), adapted from [30].

$$\frac{1}{\tau_{eff}} = \frac{1}{\tau_b} + \frac{2S_{eff}}{W} \quad (1)$$

where τ_b represents the bulk carrier lifetime and W is the thickness of the silicon sample. For samples exhibiting a sufficiently high bulk lifetime, bulk recombination has a negligible contribution to the overall recombination rate. Under this condition, recombination is dominated by surface effects, allowing the effective surface recombination velocity to be approximated using Equation (2):

$$S_{eff} = \frac{W}{2\tau_{eff}} \quad (2)$$

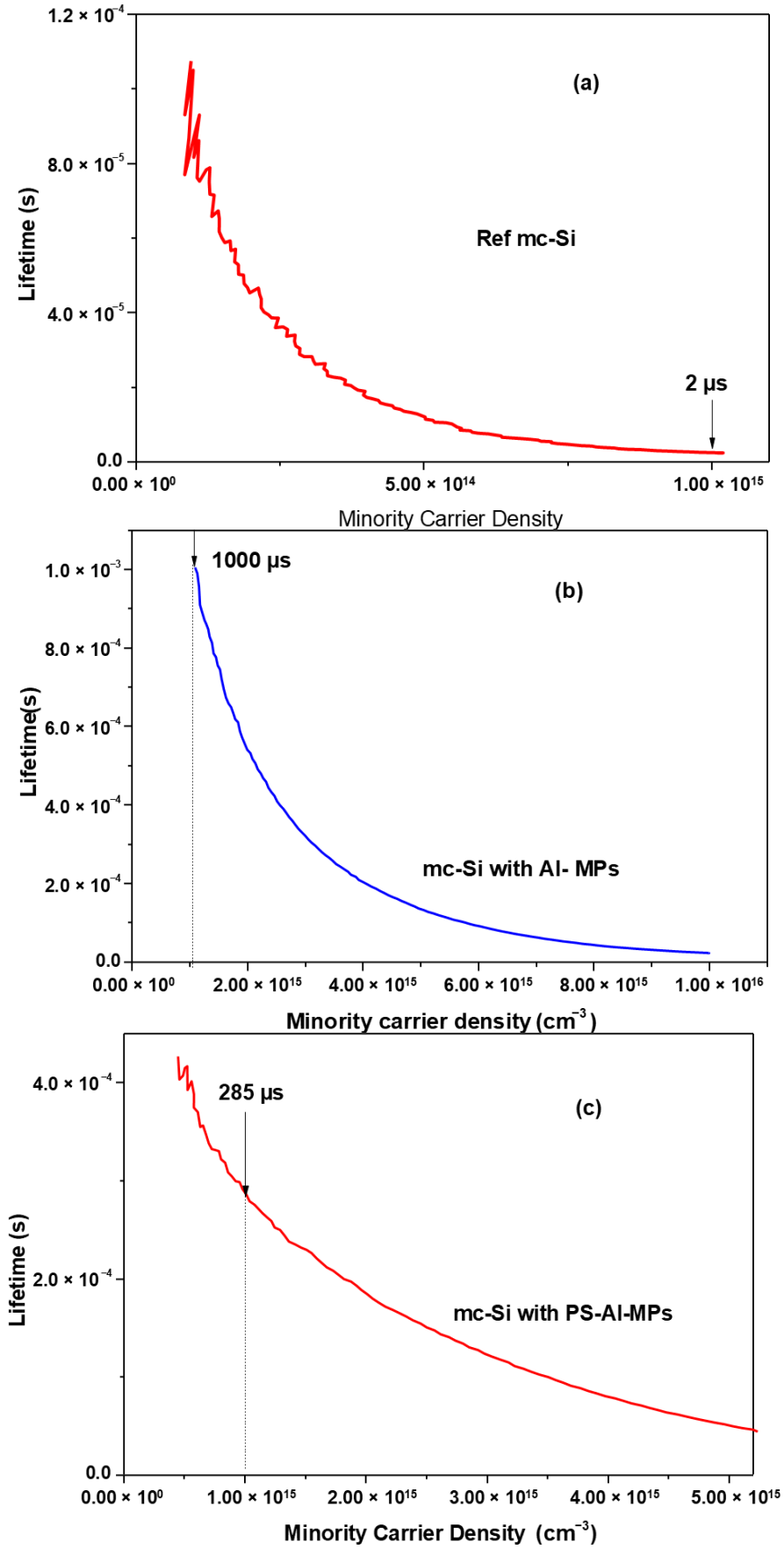

Figure 5. Effective lifetime measured under different processing, (**a**) Ref mc-Si, (**b**) mc-Si with Al-µPs and (**c**) mc-Si with PS-Al-µPs.

Table 1. Measured τ_{eff} and S_{eff} values before and after surface passivation.

	Ref mc-Si	mc-Si with Al-MPs	mc-Si with PS-Al-MPs
τ_{eff} (μs)	2	1000	285
S_{eff} ($cm \cdot s^{-1}$)	50	0.1	0.35

This approach enables a reliable evaluation of surface passivation quality and provides direct insight into the effectiveness of applied surface treatments. Table 1 summarizes the experimentally measured τ_{eff} and S_{eff} values for the samples prior to and following PS-Al-μPs surface passivation.

The formation of mc-Si/Al-μPs leads to a pronounced reduction in the effective surface recombination velocity S_{eff}, which decreases from nearly 50 $cm \cdot s^{-1}$ for the untreated sample to approximately 0.1 $cm \cdot s^{-1}$. In addition, the electronic quality of the samples is further improved after the PS–Al–μPs treatment is carried out using the stain-etching technique. The applied surface modification yields an effective surface recombination velocity of approximately 0.35 $cm \cdot s^{-1}$, which is lower than the values reported for silicon surfaces passivated using double-sided ALD-grown Al_2O_3 layers [31]. This result indicates an efficient suppression of carrier recombination at the silicon surface and highlights the effectiveness of the proposed passivation method.

The improvement in minority carrier lifetime, along with the decrease in effective surface recombination velocity observed after PS–Al–μPS treatment of mc-Si, is mainly associated with the formation of Al–O–Si, Al–O, and Si–H bonds [32–36]. FTIR spectroscopy (Figure 6) confirms the presence of these bonds through characteristic absorption peaks assigned to Si–H, Al–O, Al–O–Si, and Si–O–Si vibrations [37–40], appearing at approximately 480 cm^{-1}, 600–650 cm^{-1}, 803 cm^{-1}, and 1090 cm^{-1}, respectively. The formation of these chemical bonds contributes to effective passivation of the PS/Si interface, thereby reducing surface recombination. In addition, the Energy-Dispersive X-ray Spectroscopy (EDS) spectrum, as shown in Figure 6c, confirms the composition of the Al-etched porous silicon, showing a dominant Si peak at ~1.74 keV and a smaller Al peak at ~1.49 keV from residual aluminum. A minor O signal (~0.52 keV) corresponds to surface oxidation or the native oxide layer. The absence of significant impurity peaks indicates a high-purity porous structure, consistent with the observed morphology.

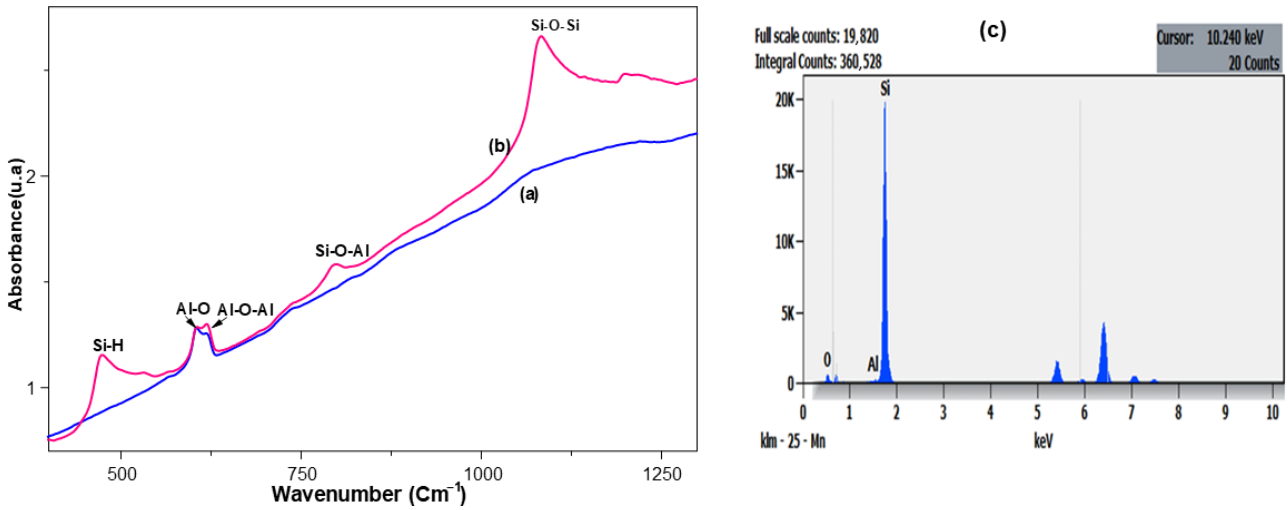

Figure 6. FTIR spectrum of mc-Si (**a**) Al-μPs and (**b**) PS-Al-μPs and (**c**) EDX.

Furthermore, annealing at 700 °C facilitates the diffusion of aluminum along the wafer surface, creating trapping sites capable of capturing recombination-active impurities while simultaneously generating a high density of fixed negative charges [41]. This phenomenon is also partly linked to internal gettering processes, including the precipitation of SiO_2 and the formation of stable impurity complexes such as $FeSi_2$ and FeB, which help decrease the concentration of recombination centers within the silicon bulk. Consequently, these combined effects contribute to a longer carrier lifetime and improved electrical quality of the silicon substrate [22].

Optical characterization of the mc-Si surface was performed via reflectivity measurements. Figure 7 shows the reflectance spectra of the mc-Si substrates before and after dual treatment. PS naturally exhibits low reflectivity due to its high surface roughness and graded refractive index. In addition, their combination with Al-μPs significantly enhances light absorption by increasing photon scattering and extending the effective optical path length. The pore morphology is particularly effective at trapping light and reducing surface reflectivity at shorter wavelengths, lowering reflectance below 9% across most of the 300–1200 nm spectrum and reaching approximately 6% in the 300–400 nm range. The average reflectance decreases from 34.6% before treatment to about 9.1% over 400–800 nm (Figure 4). In addition, aluminum passivation of grain boundaries reduces defect-induced recombination. While the minority carrier lifetime is moderately reduced, the combined effect of enhanced light trapping and lower reflectance demonstrates the surface's strong potential for photovoltaic applications, where efficient light harvesting is crucial for device performance.

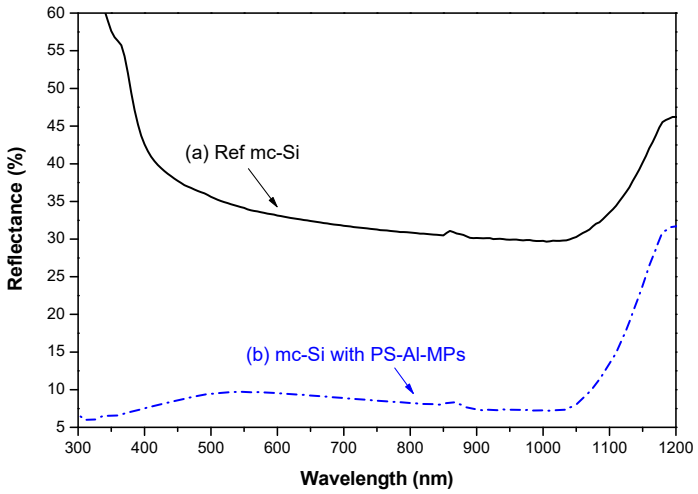

Figure 7. Variation in the surface reflectivity of mc-Si before and after PS-Al-μPs treatment.

High-resolution maps of the interstitial iron concentration ($[Fe_i]$) before and after treatment of mc-Si PS-Al-μPs were obtained using a WT-2000PVN Multifunction Wafer Mapping Tool. The system utilizes a 904 nm laser, enabling carrier excitation to a depth of approximately 30 μm within the silicon substrate and allowing spatially resolved evaluation of the bulk iron distribution and its evolution following treatment. In mc-Si, assessing the bulk effect of a treatment involves determining how processes such as Al-μPs gettering at the annealing temperature modify the internal material properties, particularly through the reduction in interstitial iron and associated recombination-active defects. The effectiveness of the treatment is primarily evaluated by quantifying changes in the interstitial iron concentration across the wafer, thereby verifying improvements in the electronic quality of the silicon and enabling precise spatial characterization of $[Fe_i]$. Two-dimensional mappings of the interstitial iron concentration ([Fe]) were used to assess the gettering efficiency of PS-Al-MPs on multicrystalline silicon (mc-Si), as shown in Figure 8. Compared with the

untreated substrate, PS-Al-MPs treatment induces a pronounced redistribution and overall reduction in [Fe], particularly at the wafer edges where iron accumulation was initially highest. Before treatment, [Fe] values ranged from (2.9–7.8) $\times$ 10^{12} cm^{-3}. After treatment, the concentration decreased across the entire wafer to (2.1–6.7) $\times$ 10^{12} cm^{-3}. This corresponds to a reduction of approximately 14–28% across the wafer, with the strongest improvement observed at the edges. This decrease in [Fe] is accompanied by an enhancement of the effective carrier lifetime, indicating efficient impurity passivation mediated by PS-Al-MPs. The elevated iron concentration in the untreated mc-Si, especially near the edges, is attributed to iron incorporation during directional solidification. The marked reduction in [Fe] after treatment confirms the effectiveness of the PS-Al-MPs gettering process in suppressing iron-related contamination.

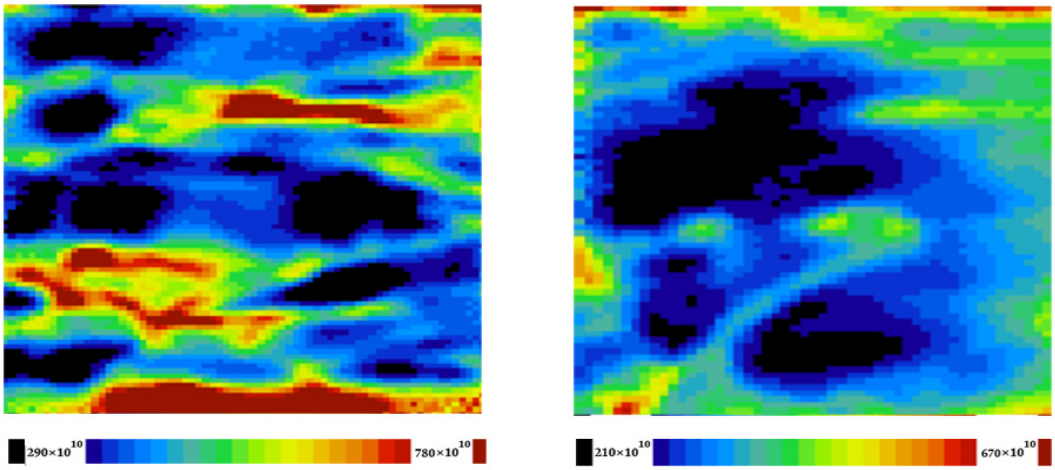

Figure 8. Interstitial iron concentration (Fe) of mc-Si before and after PS-Al-μPs treatment.

The simultaneous enhancement of optical absorption, minority carrier lifetime, and surface properties underscores the potential of PS/Al-μPs composites as an efficient, scalable platform for silicon-based optoelectronic applications. Increased light absorption is primarily attributed to enhanced light confinement and suppressed reflectance. Furthermore, the extension of carrier lifetime indicates a reduction in recombination processes, likely resulting from effective surface passivation and a lower defect density. The improved surface homogeneity further facilitates more efficient transport and collection. Collectively, these attributes position PS/Al-μPs composites as promising candidates for high-performance photovoltaics and photo detectors. Future optimization of material stoichiometry and microstructural morphology, alongside integration into functional device architectures, may further enhance performance and enable large scale implementation.

4. Conclusions

In summary, the mc-Si with PS/Al-μPs composite provides a highly effective surface modification for multicrystalline silicon, simultaneously enhancing optical and electronic performance. Surface reflectance was reduced from 34.6% to 9.1%, demonstrating superior light-trapping efficiency. Minority carrier lifetime increased dramatically from 2 μs in untreated mc-Si to 285 μs after PS/Al-μPs treatment, reflecting significant suppression of recombination. Correspondingly, the effective surface recombination velocity decreased from 50 $cm{\cdot}s^{-1}$ to 0.35 $cm{\cdot}s^{-1}$, and a reduction in [Fe] after treatment confirms the effectiveness of the PS-Al-μPs gettering process in suppressing iron-related contamination, indicating highly efficient surface passivation. These combined improvements in optical absorption, carrier lifetime, and surface quality confirm the potential of PS/Al-μPs composites as a

scalable and versatile platform for high-efficiency photovoltaic cells, photo detectors, and other silicon-based optoelectronic devices.

Author Contributions: All authors contributed to this study's conception and design. Conceptualization, Y.Z. and M.B.R.; methodology, Y.Z.; software, W.D.; validation, M.B.R., W.D. and Y.Z.; formal analysis, A.M.; investigation, R.B.Z.; resources, M.A.A.; data curation, R.B.Z.; writing—original draft preparation, A.M. and M.A.A.; writing—review and editing, A.M.; visualization, K.C.; supervision, M.B.R.; project administration, K.C.; funding acquisition, K.C. All authors have read and agreed to the published version of the manuscript.

Funding: This work was supported and funded by the Deanship of Scientific Research at Imam Mohammad Ibn Saud Islamic University (IMSIU) (grant number IMSIU-DDRSP2602).

Data Availability Statement: The original contributions presented in the study are included in the article; further inquiries can be directed to the corresponding author.

Conflicts of Interest: The authors declare no conflicts of interest.

References

1. Izam, N.S.M.N.; Itam, Z.; Sing, W.L.; Syamsir, A. Sustainable Development Perspectives of Solar Energy Technologies with Focus on Solar Photovoltaic—A Review. *Energies* **2022**, *15*, 2790. [CrossRef]
2. Wang, A.; Lin, Q.; Liu, C.; Yang, L.; Sun, S. Sustainable Energy Development: Reviewing Carbon Emission Reduction in Photovoltaic Power Systems. *Sustainability* **2024**, *16*, 10428. [CrossRef]
3. Liu, D.; Liu, J.; Wang, S.; Xu, M.; Akbar, S.J. Contribution of international photovoltaic trade to global greenhouse gas emission reduction: The example of China. *Resour. Conserv. Recycl.* **2019**, *143*, 114–118. [CrossRef]
4. Burtescu, S.; Parvulescu, C.; Babarada, F.; Manea, E. The low cost multicrystalline silicon solar cells. *Mater. Sci. Eng. B* **2009**, *165*, 190–193. [CrossRef]
5. Lan, C.W.; Hsu, C.; Nakajima, K. Multicrystalline silicon crystal growth for photovoltaic applications. In *Handbook of Crystal Growth*; Elsevier: Amsterdam, The Netherlands, 2015; pp. 373–411.
6. Lv, X.; Li, H.; Ding, D.; Yu, X.; Jin, C.; Yang, D. Interfacial characterization of non-metal precipitates at grain boundaries in cast multicrystalline silicon crystals. *J. Cryst. Growth* **2025**, *652*, 128042. [CrossRef]
7. Wang, L.; Liu, J.; Li, Y.; Wei, G.; Li, Q.; Fan, Z.; He, D. Dislocations in Crystalline Silicon Solar Cells. *Adv. Energy Sustain. Res.* **2024**, *5*, 2300240. [CrossRef]
8. Chen, J.; Chen, B.; Lee, W.; Fukuzawa, M.; Yamada, M.; Sekiguchi, T. Grain boundaries in multicrystalline si. *Solid State Phenom.* **2010**, *156*, 19–26. [CrossRef]
9. Woo, S.; Bertoni, M.; Choi, K.; Nam, S.; Castellanos, S.; Powell, D.M.; Choi, H. An insight into dislocation density reduction in multicrystalline silicon. *Sol. Energy Mater. Sol. Cells* **2016**, *155*, 88–100. [CrossRef]
10. Alrasheedi, N.H. The effects of porous silicon and silicon nitride treatments on the electronic qualities of multicrystalline silicon for solar cell applications. *Silicon* **2024**, *16*, 1765–1773. [CrossRef]
11. Almeshaal, M.A.; Abdouli, B.; Choubani, K.; Khezami, L.; Rabha, M.B. Study of porous silicon layer effect in optoelectronics properties of multi-crystalline silicon for photovoltaic applications. *Silicon* **2023**, *15*, 6025–6032. [CrossRef]
12. Ogundipe, O.B.; Okwandu, A.C.; Abdulwaheed, S.A. Recent advances in solar photovoltaic technologies: Efficiency, materials, and applications. *GSC Adv. Res. Rev.* **2024**, *20*, 159–175. [CrossRef]
13. Mohd Nasir, N.S.; Mohd Rais, A.R.; Mohd Sinin, N.A.; Sopian, K. Surface Quality Optimisation of Monocrystalline and Polycrystalline Silicon Wafers through Cleaning, Etching and Texturisation Processes for Si Solar Cell Applications. *J. Phys. Sci.* **2025**, *36*, 39–59. [CrossRef]
14. Dasilva-Villanueva, N.; Catalán-Gómez, S.; Marrón, D.F.; Torres, J.J.; García-Corpas, M.; del Cañizo, C. Reduction of trapping and recombination in upgraded metallurgical grade silicon: Impact of phosphorous diffusion gettering. *Sol. Energy Mater. Sol. Cells* **2022**, *234*, 111410. [CrossRef]
15. Porre, O.; Martinuzzi, S.; Pasquinelli, M.; Perichaud, I.; Gay, N. Gettering effect of aluminium in mc-Si and c-Si wafers and in solar cells. In Proceedings of the Conference Record of the Twenty Fifth IEEE Photovoltaic Specialists Conference, Washington, DC, USA, 13–17 May 1996.
16. Achref, M.; Bessadok, A.J.; Khezami, L.; Mokraoui, S.; Benrabha, M. Effective surface passivation on multi-crystalline silicon using aluminum/porous silicon nanostructures. *Surf. Interfaces* **2020**, *18*, 100391. [CrossRef]

17. Liu, A.; Sun, C.; Sio, H.C.; Zhang, X.; Jin, H.; Macdonald, D. Gettering of Transition Metals in High-Performance Multicrystalline Silicon by Silicon Nitride Films and Phosphorus Diffusion. *J. Appl. Phys.* **2019**, *125*, 043103. [CrossRef]
18. Sun, C.; Liu, A.; Samadi, A.; Chan, C.; Ciesla, A.; Macdonald, D. Transition Metals in a Cast-Monocrystalline Silicon Ingot Studied by Silicon Nitride Gettering. *Phys. Status Solidi RRL* **2019**, *13*, 1900456. [CrossRef]
19. Amri, C.; Ouertani, R.; Hamdi, A.; Ezzaouia, H. Enhancement of electrical parameters in solar grade monocrystalline silicon by external gettering through sacrificial silicon nanowire layer. *Mater. Res. Bull.* **2018**, *98*, 41–46. [CrossRef]
20. Dimassi, W.; Bouaïcha, M.; Kharroubi, M.; Lajnef, M.; Ezzaouia, H.; Bessaïs, B. Two-dimensional LBIC and internal quantum efficiency investigations of porous silicon-based gettering procedure in multicrystalline silicon. *Sol. Energy Mater. Sol. Cells* **2008**, *92*, 1421–1424. [CrossRef]
21. Ben Rabha, M.; Belhadj Mohamed, S.; Hajjaji, A.; Dimassi, W.; Hajji, M.; Aouida, S.; Gaidi, M.; Bouaicha, M.; Bessais, B. Minority carrier lifetime enhancement in multicrystalline silicon. *Eur. Phys. J. Appl. Phys.* **2012**, *57*, 21302. [CrossRef]
22. Litovchenko, V.G.; Naseka, V.M.; Evtukh, A.A. Two-channel gettering of recombination-active impurity in polycrystalline solar silicon. *Ukr. J. Phys.* **2012**, *57*, 73–79.
23. Mogoda, A.S.; Farag, A.R. The effects of a few formation parameters on porous silicon production in HF/HNO_3 using ag-assisted etching and a comparison with a stain etching method. *Silicon* **2022**, *14*, 11405–11415. [CrossRef]
24. Peng, K.; Lu, A.; Zhang, R.; Lee, S.T. Motility of metal nanoparticles in silicon and induced anisotropic silicon etching. *Adv. Funct. Mater.* **2008**, *18*, 3026–3035. [CrossRef]
25. Choubani, K.; Zouari, Y.; El Haj, A.; Mannai, A.; Almeshaal, M.A.; Dimassi, W.; Ben Rabha, M. Enhancing Optoelectronic Properties of Multicrystalline Silicon Using Dual Treatments for Solar Cell Applications. *Inorganics* **2025**, *13*, 142. [CrossRef]
26. Alsolami, A.; Hussain, H.; Noor, R.; AlAdi, N.; Almalki, N.; Kurdi, A.; Tabbakh, T.; Zaman, A.; Alfihed, S.; Wang, J. Recent Advances in Black Silicon Surface Modification for Enhanced Light Trapping in Photodetectors. *Appl. Sci.* **2024**, *14*, 9841. [CrossRef]
27. Vinod, P.N. Porous Silicon and Aluminum Co-Gettering Experiment in p-Type Multicrystalline Silicon Substrate. *Sci. Technol. Adv. Mater.* **2007**, *8*, 231–236. [CrossRef]
28. Castellanos, S.; Ekstrøm, K.E.; Autruffe, A.; Jensen, M.A.; Morishige, A.E.; Hofstetter, J.; Yen, P.; Lai, B.; Stokkan, G.; del Cañizo, C.; et al. High-performance and traditional multicrystalline silicon: Comparing gettering responses and lifetime-limiting defects. *IEEE J. Photovolt.* **2016**, *6*, 632–640. [CrossRef]
29. Vicari Stefani, B.; Weigand, W.; Wright, M.; Soeriyadi, A.; Yu, Z.; Kim, M.; Hallam, B. P-type upgraded metallurgical-grade multicrystalline silicon heterojunction solar cells with open-circuit voltages over 690 mV. *Phys. Status Solidi A* **2019**, *216*, 1900319. [CrossRef]
30. Cuevas, A.; Macdonald, D. Measuring and interpreting the lifetime of silicon wafers. *Sol. Energy* **2004**, *76*, 255–262. [CrossRef]
31. Jia, X.; Zhou, C.; Wang, W. Optimization of the Surface Structure on Black Silicon for Surface Passivation. *Nanoscale Res. Lett.* **2017**, *12*, 193. [CrossRef]
32. Roy, J.; Bandyopadhyay, N.; Das, S.; Maitra, S. Studies on the formation of mullite from diphasic Al_2O_3-SiO_2 gel by fourier transform infrared spectroscopy. *Iran. J. Chem. Chem. Eng.* **2011**, *30*, 65–71.
33. Jemai, A.B.; Mannai, A.; Khezami, L.; Mokraoui, S.; Algethami, F.K.; Al-Ghyamah, A.; Rabha, M.B. Aluminum nanoparticles passivation of multi-crystalline silicon nanostructure for solar cells applications. *Silicon* **2020**, *12*, 2755–2760. [CrossRef]
34. M'Gafad, N.; Amzil, H.; Sayah, D.; Ballutaud, D.; Barbé, M. Passivation of the grain boundary electrical activity in multicrystalline silicon: Aluminum treatment efficiency. *Solid-State Electron.* **1999**, *43*, 857–864. [CrossRef]
35. Chu, M.; Jeong, Y.; Jang, Y.; Pan, Z.; Aida, M.N.; Bae, J.; Yi, J. A novel approach for improved passivation of a-Si and a-Si/c-Si surfaces from deuterium plasma effects. *J. Phys. D Appl. Phys.* **2025**, *58*, 235104. [CrossRef]
36. Salem, M.; Massoudi, I.; Almessiere, M.A.; Al-Otaibi, A.L.; Alghamdi, N.M.; Gaidi, M.; Khirouni, K. Structural, morphological and optoelectronic properties of porous silicon combined alumina coating film deposited by PLD. *J. Mater. Sci. Mater. Electron.* **2017**, *28*, 15768–15774. [CrossRef]
37. Gentile, F.S.; Difalco, A.; Pascale, F.; Salustro, S.; Mackrodt, W.; Dovesi, R. The spectroscopic characterization of interstitial oxygen in bulk silicon: A quantum mechanical simulation. *J. Chem. Phys.* **2020**, *152*, 054502. [CrossRef] [PubMed]
38. Soule, D.E.; Reedy, G.T. Infrared spectra of the hydrogenated amorphous silicon layers on metallic substrates of solar absorbers. *Thin Solid. Film.* **1979**, *63*, 175–181. [CrossRef]
39. Beyzay, F.; Hosseini, A.Z.; Soudi, S. Alpha alumina nanoparticle conjugation to cysteine peptidase A and B: An efficient method for autophagy induction. *Avicenna J. Med. Biotechnol.* **2017**, *9*, 71.

40. Giacomazzi, L.; Shcheblanov, N.S.; Povarnitsyn, M.E.; Li, Y.; Mavrič, A.; Zupančič, B.; Pasquarello, A. Infrared spectra in amorphous alumina: A combined ab initio and experimental study. *Phys. Rev. Mater.* **2023**, *7*, 045604. [CrossRef]
41. Agostinelli, G.; Delabie, A.; Vitanov, P.; Alexieva, Z.; Dekkers, H.F.W.; De Wolf, S.; Beaucarne, G. Very low surface recombination velocities on p-type silicon wafers passivated with a dielectric with fixed negative charge. *Sol. Energy Mater. Sol. Cells* **2006**, *90*, 3438–3443. [CrossRef]

Disclaimer/Publisher's Note: The statements, opinions and data contained in all publications are solely those of the individual author(s) and contributor(s) and not of MDPI and/or the editor(s). MDPI and/or the editor(s) disclaim responsibility for any injury to people or property resulting from any ideas, methods, instructions or products referred to in the content.